Materials Chemistry and Physics 143 (2014) 707–712

Contents lists available at ScienceDirect

Materials Chemistry and Physics

journal homepage: www.elsevier.com/locate/matchemphys

Preparation and characterization of porous carbons obtained from mixtures of furfuryl alcohol and phenol–formaldehyde resin

Zhiyong Yuan*, Yumin Zhang, Yufeng Zhou, Jiecai Han

Science and Technology on Advanced Composites in Special Environments Laboratory, Harbin Institute of Technology, Harbin 150001, PR China

HIGHLIGHTS

- Varying mixture composition led phase separation dynamics to change.
- Cured samples with higher FA content had skeleton of high polymerization degree.
- Porous carbons with controlled pore structure were obtained by changing FA content.

ARTICLE INFO

Article history:
Received 14 March 2013
Received in revised form
3 September 2013
Accepted 2 October 2013

Keywords:
Polymers
Microstructure
Thermogravimetric analysis
Fourier transform infrared spectroscopy

ABSTRACT

Crosslinked carbon network with interconnected pores were obtained from [furfuryl alcohol (FA) + phenol–formaldehyde resin (PF)] – ethylene glycol (EG) mixtures. The effect of FA/PF weight ratio ($W_{F/P}$) on the pore structure of the porous carbons has been systematically investigated. The results showed that porous carbons with controlled pore size could be obtained by varying $W_{F/P}$ in the polymer system. With $W_{F/P}$ increased, the average pore size and apparent porosity increased from 11.8 to 127.7 nm and from 40.9 to 51.6%, respectively, and the pore size distribution broadened. The property change of the porous carbons was a result of polymerization dynamics change on curing of resin–glycol mixtures induced by varying $W_{F/P}$ in the polymer system. Increasing the initial $W_{F/P}$ led curing reactions to occur at relatively lower temperatures, and the degree of polymerization to increase after heat treatment at 150 °C for 16 h, thus cured bodies with different chemical structures were obtained.

1. Introduction

Porous carbon materials have received much attention due to their remarkable properties, such as high specific surface area, large pore volume, good electrical conductivity, chemical inertness and good mechanical stability [1–3]. Porous carbon materials have been applied to water and air purification, gas separation, catalyst support, chromatography, energy storage and preparation of structural carbide ceramics [4–6]. Up to now, many methods have been employed to synthesize porous carbon materials, and the most commonly used are direct carbonization of porous polymer [7,8], activation method [9,10], template method [11,12] and polymer blend carbonization method (PBC) [13–16].

Many researchers have reported the synthesis of porous carbon with controlled pore structure based on PBC, and the characteristics of the porous carbons synthesized by PBC appear to be defined by many parameters, including the specific composition of the resin mixtures and the thermal history of the polymer system [15,16]. However, few studies have addressed porous carbons based on homopolymer and monomer mixtures. Pyrolysis of monomer–homopolymer mixed system may provide carbons with modified structures and properties. Thus, the understanding of the relationship between the compositions of the starting polymer systems and the properties of the carbon materials obtained after carbonization is important to the application and modification of the carbon materials.

It has been pointed out that the morphology and pore structure of the porous carbons obtained from polymer blend carbonization method were fully developed after polymerization [15,16]. Thus, in order to exert control the pore structure of porous carbons, an adequate understanding of the polymerization process is very necessary. However, few studies have addressed the possible polymerization of furfuryl alcohol (FA)/phenolic resin (PF)/ethylene glycol (EG) mixtures under an acid condition, and the possible relations between polymerization process and pore structure of carbonized products. In this paper, FA/PF/EG mixtures were used to prepare porous carbon through PBC, and the influence of $W_{F/P}$ on the polymerization of the resin mixtures and the pore structure of the porous carbons is investigated, with emphasis on

* Corresponding author. Tel./fax: +86 0451 86403849.
E-mail addresses: yuanzy_1986@163.com, zhiyyuan@yahoo.cn (Z. Yuan).

0254-0584/$ – see front matter © 2013 Elsevier B.V. All rights reserved.
http://dx.doi.org/10.1016/j.matchemphys.2013.10.001

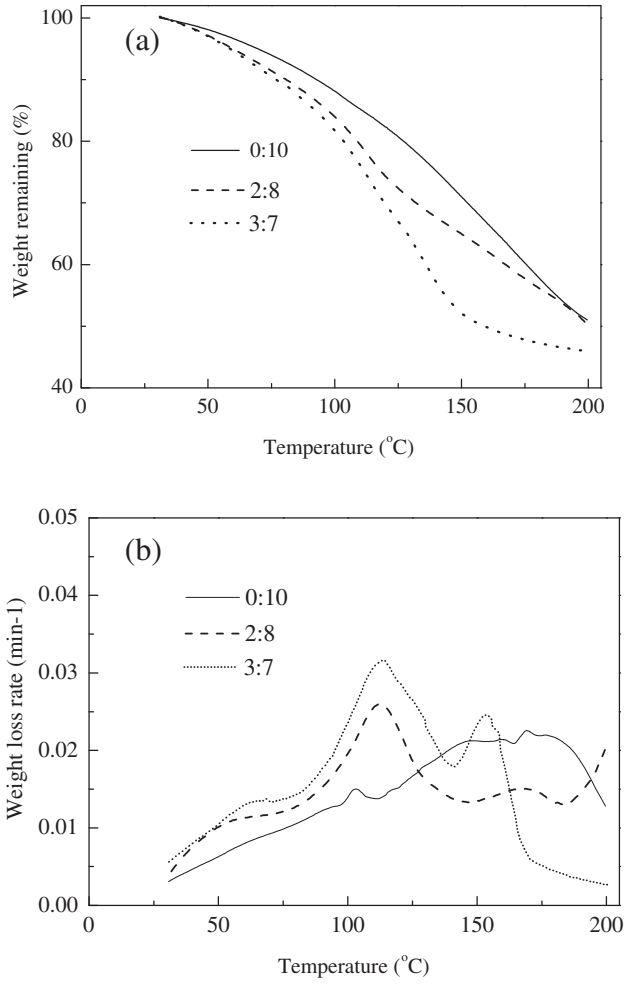

Fig. 1. Influence of $W_{F/P}$ on TG curves during polymerization: (a) weight loss curves; (b) weight loss rate curves.

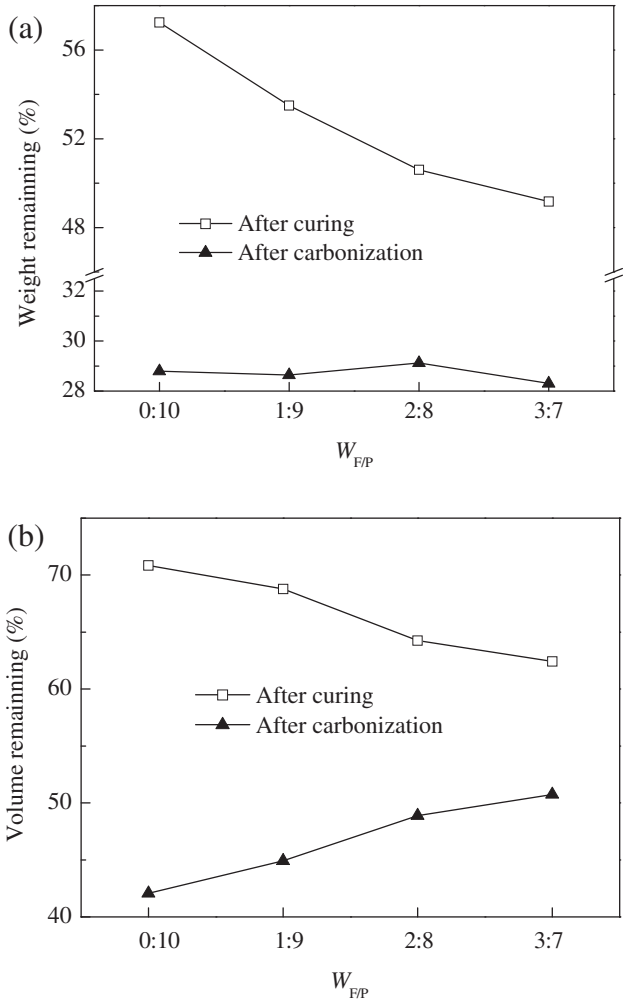

Fig. 2. The effect of $W_{F/P}$ on weight (a) and volume (b) change of samples after curing and pyrolysis.

understanding and controlling the polymerization reactions of the resin mixtures and the morphology, average pore size, apparent porosity and pore size distribution of the porous carbons.

2. Experimental section

2.1. Sample preparation

Resol-type PF #2130 was prepared from a condensation polymerization reaction of phenol and excess formaldehyde using sodium carbonate (Na_2CO_3) as the catalyst, and was used without further purification. At first, PF, FA, EG and benzenesulfonyl chloride were mixed by stirring mechanically for 30 min at room temperature. Then the resin mixtures were heated up to 150 °C and held for 16 h to finish curing. The cured samples were pyrolyzed by slowly ramping to 800 °C in a flowing nitrogen atmosphere, followed by cooling naturally to room temperature. Four specimens were prepared, and the $W_{F/P}$ was 0:10, 1:9, 2:8 and 3:7, respectively. The resulting porous carbons were designated as PC1, PC2, PC3 and PC4, accordingly.

2.2. Characterization

The weight loss behaviors of the resin mixtures during polymerization were measured in flowing argon using a thermobalance (TGA/SDTA85IE, Switherland). The heat rate and final temperature were 5 °C min^{-1} and 200 °C. Weight and volume changes of the samples after curing and pyrolysis were determined from the change in weight and volume between pre-curing and final

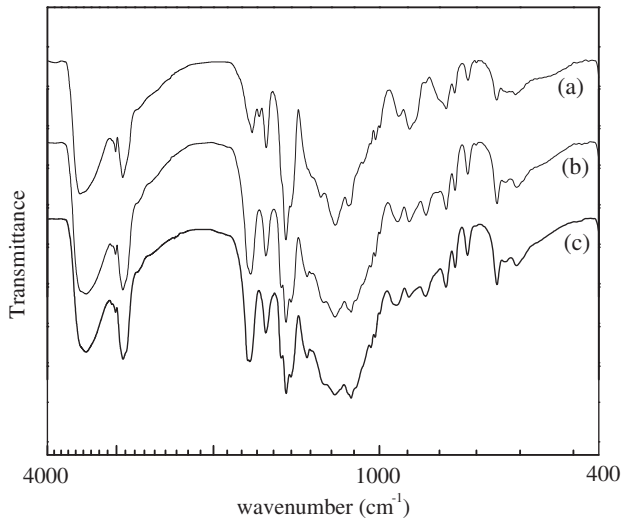

Fig. 3. FT-IR spectra of the cured samples with different $W_{F/P}$: (a) 0:10; (b) 2:8; (c) 3:7.

Table 1
Peak assignment of FT-IR spectra of the cured samples.

Wavenumber (cm^{-1})	Functional group
3500–3200	O–H stretching
3100–2800	C–H stretching (>3000, aromatic C–H;<3000, aliphatic C–H)
1730–1650	C=O stretching
1600	C–C stretching of aromatic ring
1477	C–H bending of aliphatic bridge structure
1445	C–O–C stretching of dibenzyl ether linkages
1277	C–O stretching of diphenyl ether structure
1200	C–O stretching of phenol group
881, 823, 757	C–H out-of-plane deformation vibrations of benzene ring substitution

samples. The Fourier transform infrared spectra (FT-IR) of the cured bodies were obtained using the KBr pellet technique from a Fourier transform infrared spectrometer (Spectrum One B, USA) in the wavenumber range of 4000–400 cm^{-1} at a resolution of 1 cm^{-1}.

The morphologies of the cured samples and porous carbons were examined with a field emission scanning electron microscopy (QUANTA 200, FEI, USA). Pore structure of the carbonized products was examined by a mercury porosimetry (Micromeritics, PoreSizer 9500, USA). The surface areas and the pore structures of samples with average pore sizes <100 nm were determined from nitrogen adsorption–desorption isotherms (Micromertics, ASAP 2010, USA). The resulting isotherms were analyzed using the Brunaur–Emmett–Teller (BET) method, and pore size distributions were carried out using the Barrett–Joyner–Halenda (BJH) method. Before the measurement, all samples were degassed under vacuum at 150 °C for 180 min.

3. Results and discussion

3.1. Interactions between FA and PF

3.1.1. Thermogravimetric analysis

The thermogravimetric curves of the resin mixtures with different $W_{F/P}$ during polymerization are shown in Fig. 1. It is clear that the rate of polymerization is significantly influenced by the $W_{F/P}$ in the starting resin mixture. When the resin mixture consists of only PF and EG, the rate of polymerization is very slow, and the weight loss rate of the resin mixtures slowly increases with temperature, with the distinct peak of weight loss rate appearing at about 150–180 °C. When PF is partly substituted by FA, however, a runaway exothermic reaction followed by rapid solidification tends to occur, and the weight loss rate has three distinct peaks. The first peak, appearing at about 65 °C, with its peak value increasing with increased $W_{F/P}$, can be assigned to the reaction between hydroxymethylol (from PF and FA) and hydrogen ions (from the hydrolysis of benzenesulfonyl chloride) to form some intermediates and water [17,18]. The second peak at about 110 °C is mainly due to the chemical reactions between the intermediates [19]. The third peak, which shifts to lower temperatures with higher $W_{F/P}$, is due to the evaporation of EG.

According to Xu [15], continuous and dispersed EG-rich phase are both formed during phase separation, and the continuous EG-rich phase is nearly removed during curing, while the dispersed one is removed during pyrolysis. Fig. 2 illustrates the weight and volume change of samples with different $W_{F/P}$ after curing and pyrolysis. It is clear that the remaining weight of the samples after cured at 150 °C for 16 h decreases gradually with increasing $W_{F/P}$, while that after carbonized at 800 °C can be steadied in range from 28.3 to 29.2%. It is concluded that the amount of dispersed EG-rich

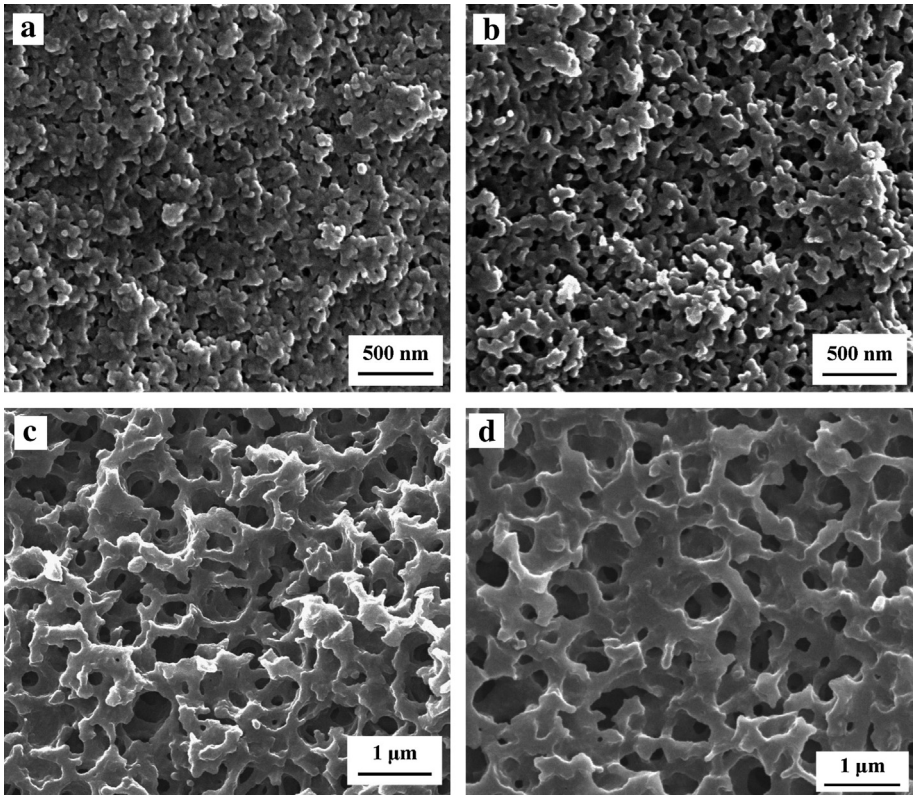

Fig. 4. Morphological changes of the porous carbons with different $W_{F/P}$: (a) PC1; (b) PC2; (c) PC3; (d) PC4.

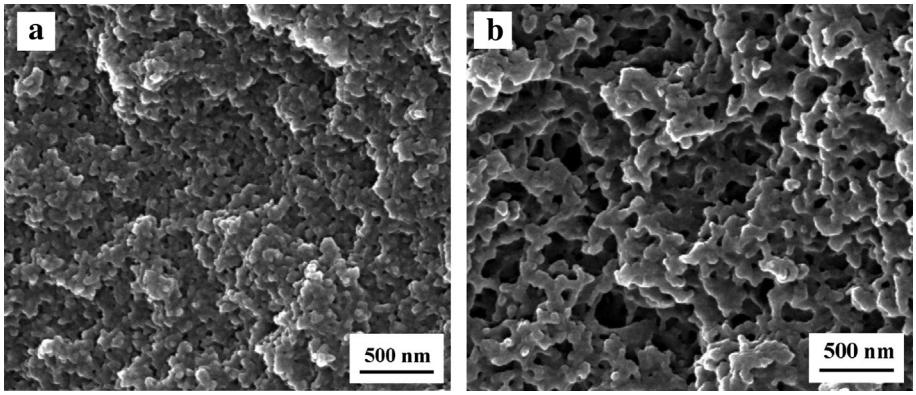

Fig. 5. Morphologies of the curried bodies with different $W_{F/P}$: (a) 0:10; (b) 2:8.

phase in the cured bodies with higher $W_{F/P}$ is less than that with lower $W_{F/P}$. Fig. 2 also shows that less FA leads to more serious volume shrinkage after pyrolysis.

3.1.2. FT-IR spectra analysis

The FT-IR spectra of cured samples were used to identify the intermediate structures present after the polymerization of the resin mixtures. Fig. 3 shows the FT-IR spectra of the cured bodies with different $W_{F/P}$. Following recognized peak identification of infrared spectra of PF and FA [20–25], functional groups corresponding to the major bands of the spectra have been assigned as listed in Table 1. Comparison of the spectra of samples with different $W_{F/P}$ in Fig. 3 shows that there are several remarkable differences, summarized as follows:

(a) The band at 1477 cm^{-1} attributed to a C–H deformation mode severely decreased in intensity with increasing of $W_{F/P}$, and that intensity decrease was paralleled by a decrease in intensity of a band near 2920 cm^{-1}, indicating an increased concentration of 1,2,4,6 tetra- and other high benzene ring substitutions [20]. Also typical of such substitutions was a band near 880 cm^{-1} due to out-of-plane C–H deformation. The spectra in the 1170–1120 cm^{-1} region became more complex (Fig. 3d), probably due to the growth of new aromatic C–H deformation bands in this region. The absorption peaks at 757 and 727 cm^{-1} were identified as resulting from 1,2 di- or 1,2,6 tri-substituted benzene ring.

On combining the above information, the polymerization degree of the resin mixtures after curing, increased with increasing $W_{F/P}$, according with the thermogravimetric analysis. Moreover, the cured bodies derived from mixtures without FA had a prevalence of 1,2,6 trisubstitutions in the chain structure, and 1,2 disubstitutions in the chain terminations. On the contrary, the cured materials prepared from mixtures with higher FA content had a prevalence of 1,2,4,6 tetra- and other high benzene ring substitutions along with 1,2,4 and 1,2,6 trisubstitutions.

(b) The broad band at 3500 cm^{-1} (O–H group) became weakened as the weight ratio of FA to PF increased from 0:10 to 3:7 The absorption peak near 1270 cm^{-1} disappeared in Fig. 3c and d, indicating disappearance of diphenyl ether linkages. The band near 1200 cm^{-1} increased in intensity with an increase of $W_{F/P}$, representing an increased concentration of C–O stretching of phenol group. The newly formed absorption peak at near 1350 cm^{-1} in Fig. 3b, c and d was assigned to the ring stretching modes of 2-substituted furan rings [21]. These results indicated that FA reacted with PF during curing of the resin mixtures, and resulted in linkages between PF and FA. Moreover, cross-reaction between PF and FA was dominant in the resin mixture [19].

Table 2
The properties of porous carbons.

Sample	Apparent porosity (%)	Average pore size (nm)	V_{total} ($cm^3\ g^{-1}$)	Bulk density ($g\ cm^{-3}$)
PC1	40.9	11.8	0.51	0.80
PC2	47.2	18.0	0.67	0.70
PC3	49.8	53.8	0.75	0.66
PC4	51.6	127.7	0.77	0.67

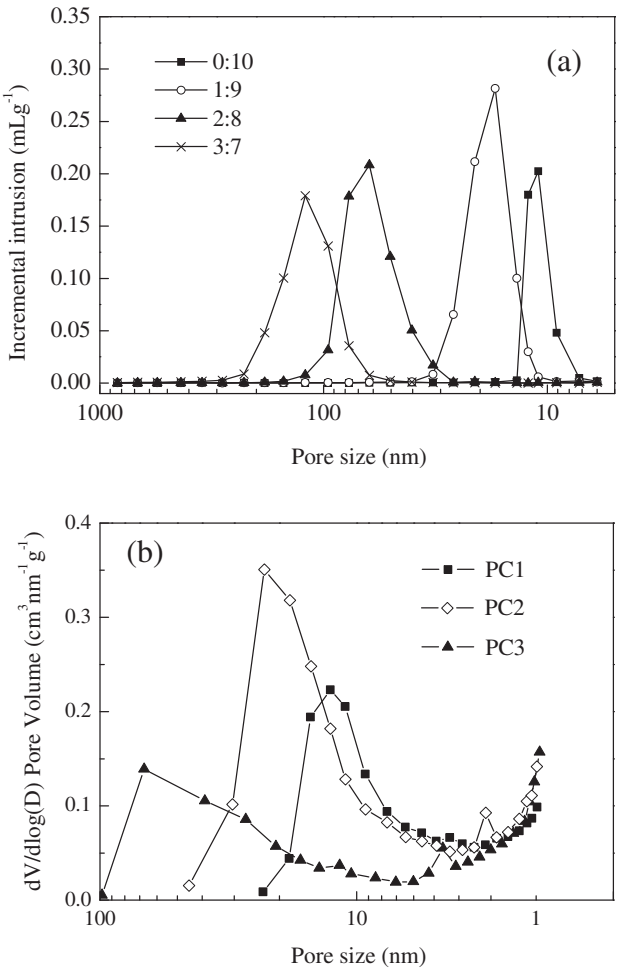

Fig. 6. Pore size distribution of the porous carbons deduced from (a) mercury porosimetry and (b) nitrogen adsorption isotherms.

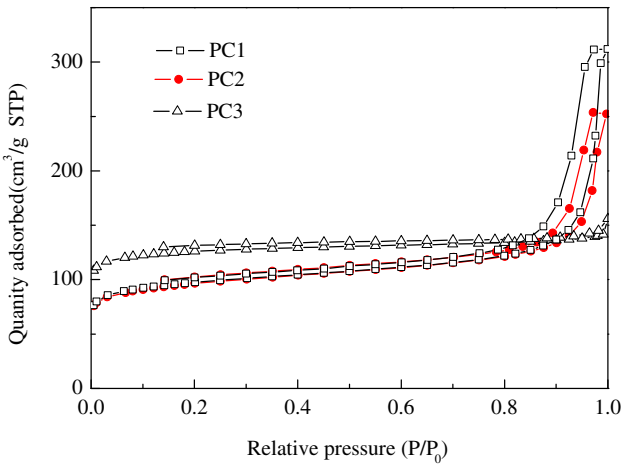

Fig. 7. Adsorption isotherms of nitrogen on carbons.

3.2. Characterization of the porous carbons

The micrographs of the porous carbons prepared from resin mixtures with different $W_{F/P}$ are illustrated in Fig. 4. It is evident that no matter what the $W_{F/P}$ was, a carbon network with interconnected pores was obtained, indicating that phase separation occurs in the course of polymerization, and continuous EG-rich phase, which endowed effective channels for removing the solvent and volatile polycondensation products during curing and subsequent pyrolysis, was formed in all the samples [15]. Carbonization of such a polymer blend will lead to the formation of porous structure, since the thermally unstable component will decompose to leave pores in the carbon matrix. Fig. 4 also shows that the carbonized resins with higher FA content had thicker carbon skeleton and bigger pore size, which could be proved by mercury porosimetry.

Fig. 5 shows the morphologies of the cured bodies (before pyrolysis). No significant morphological differences were detected in the samples before and after pyrolysis. This indicates that the morphological type of the porous carbon was fully developed after polymerization. Since the morphological type of carbonized products was inherited from that of cured bodies, varying FA content in the resin mixtures was expect to change the pore structure of resulting porous carbons by changing polymerization dynamics on curing of resin–glycol mixtures [15]. After curing, the polymerization degree of the resin mixtures increased with increased $W_{F/P}$, thus the samples obtained from resin mixtures with higher FA content had stronger ability to withstand contraction under same condition of pyrolysis (see Fig. 2), which had certain effect on the pore structure (pore size and apparent porosity) of the corresponding porous carbons. Moreover, an analysis of Figs. 1 and 2 shows that resin mixtures with higher $W_{F/P}$ have a relatively high rate of removing volatile polycondensation products and the solvent (ethylene glycol) during the formation of the cured samples, which further leads to bigger pore size and higher apparent porosity [26].

The average pore size, apparent porosity and bulk density of the porous carbons as a function of $W_{F/P}$ are determined by mercury porosimetry. The average pore size could be controlled in a wide range from 11.8 to 127.7 nm, and the average pore size of the porous carbon monoliths increased rapidly with increasing FA content, as shown in Table 2, according with observation of morphologies (Fig. 4). Table 2 also shows that the apparent porosity of the carbonized products gradually increased from 40.9 to 51.6% with increased $W_{F/P}$. The bulk density of PC1 (0.8 g cm^{-3}) was obviously higher than that of PC2 (0.7 g cm^{-3}), PC3 (0.66 g cm^{-3}) and PC4 (0.67 g cm^{-3}), which could be ascribed to the relatively low apparent porosity.

Fig. 6a demonstrates the pore size distribution of carbonized products deduced from mercury porosimetry. Without FA (PC1), the pore size distribution of carbon monoliths was very narrow, with most of pores ranging from 6 to 15 nm. The pore size distributions of porous carbons with higher FA content were broader. And when $W_{F/P}$ was 3:7 (PC4), carbonized products had pore size of 62–113 nm. Fig. 6b presents the pore size distributions of carbonized products obtained from nitrogen adsorption isotherms. An analysis of Fig. 6a and b shows that pore size distributions of samples PC1, PC2 and PC3 deduced from mercury porosimetry data agreed basically with those from nitrogen adsorption isotherms.

Fig. 7 shows the nitrogen adsorption isotherms for PC1 to PC3 obtained from an adsorption instrument. It is clear that all the samples with average pore size <100 nm exhibit type IV isotherms, characteristic features of the isotherms were its hysteresis loop, which were typical of mesoporous carbons [27]. From analysis of Figs. 4–7 and Table 1, we can safely draw a conclusion that PC1 to PC3 were confirmed to be mesoporous carbons.

4. Conclusion

The polymerization process of the resin mixtures with different $W_{F/P}$ is investigated. The results show that varying FA content in the resin mixtures led polymerization dynamics to change on curing of resin–glycol mixtures. Resin mixtures containing higher FA content undergo a relatively fast polymerization reaction and the polymerization occurs at relatively lower temperatures. Increasing $W_{F/P}$ leads the polymerization degree of the resin system to increase, and cured bodies with different chemical structures are obtained. The results also show that the morphologies of porous carbons were fully developed after polymerization, and porous carbons with different morphologies, pore size, apparent porosity and bulk density can be obtained by changing $W_{F/P}$.

Acknowledgments

This work was supported by Postdoctoral Science Foundation of China (201003435) and Key Laboratories Foundation of China (9140C49203110C4901).

References

[1] A. Stein, Z. Wang, M.A. Fierke, Adv. Mater. 21 (2009) 265–293.
[2] M. Ojima, S. Hiwatashi, H. Araki, A. Fujii, M. Ozaki, K. Yoshino, Appl. Phys. Lett. 88 (2006) 053103–053106.
[3] R. Leboda, J. Skubiszewska-Zieba, W. Grzegorczyk, Carbon 36 (1998) 417–425.
[4] B. Kim, Y. Lee, S. Park, Int. J. Hydrogen Energy 33 (2008) 2254–2259.
[5] Z. Gu, B. Deng, Environ. Eng. Sci. 24 (2007) 113–121.
[6] J. Yang, X. Zhou, J. Li, Y. Zou, J. Tang, Mater. Chem. Phys. 135 (2012) 445–450.
[7] C. Zou, D. Wu, M. Li, Q. Zeng, F. Xu, Z. Huang, et al., J. Mater. Chem. 20 (2010) 731–735.
[8] A.M. Elkhatat, S.A. Al-Muhtaseb, Adv. Mater. 23 (2011) 2887–2903.
[9] H. Teng, S. Wang, Ind. Eng. Chem. Res. 39 (2000) 673–678.
[10] M. Wu, Q. Zha, J. Qiu, X. Han, Y. Guo, Z. Li, et al., Fuel 8 (2005) 1992–1997.
[11] R. Ryoo, S.H. Joo, M. Kruk, M. Jaroniec, Adv. Mater. 13 (2001) 677–681.
[12] J. Lee, J. Kim, T. Hyeon, Chem. Commun. 15 (2003) 1138–1139.
[13] J. Ozaki, N. Endo, W. Ohizumi, K. Igarashi, M. Nakahara, A. Oya, Carbon 35 (1997) 1031–1033.
[14] Y.X. Wang, S.H. Tan, D.L. Jiang, X.Y. Zhang, Carbon 41 (2003) 2065–2072.
[15] S. Xu, J. Li, G. Qiao, H. Wang, T. Lu, Carbon 47 (2009) 2103–2111.
[16] X. Xia, H. Liu, Y. He, L. Shi, H. Chen, L. Yang, J. Iran Chem. Soc. 9 (2012) 545–550.
[17] T. Horikawa, K. Ogawa, K. Mizuno, J. Hayashi, K. Muroyama, Carbon 41 (2003) 465–472.
[18] G.M.G. Maldonado, R.S. Assary, J. Dumesic, L.A. Curtiss, Energy Environ. Sci. 5 (2012) 6981–6989.
[19] X. Zhang, D.H. Solomon, Chem. Mater. 10 (1998) 1833–1840.
[20] C. Morterra, M. Low, Carbon 23 (1985) 525–530.

[21] C. Mealares, Z. Hui, A. Gandini, Polymers 37 (1996) 2273–2279.
[22] T.C. Robert, M. Ignatius, J. Appl. Polym. Sci. 7 (1963) 1083–1091.
[23] A. Kimberly, E. Tony, Carbon 32 (1995) 1509–1515.
[24] C. Mekki, M. Naceur, G. Alessandro, Macromolecules 29 (1996) 3839–3850.
[25] Z. Wang, Z. Lu, X. Huang, R. Xue, L. Chen, Carbon 36 (1998) 51–59.
[26] S.S. Michael, A. Hans, P. Hohn, R. Dennis, C.F. Henry, Carbon 41 (2003) 2501–2508.
[27] K.S.W. Sing, D.H. Everett, R.A.W. Haul, L. Moscou, R.A. Pierotti, J. Rouquerol, et al., Pure Appl. Chem. 57 (1985) 603–619.